LA-UR -77-1028

TITLE: Neutron Cross Section Programs in the Energy Region from 1 to 24 MeV at the LASL Van de Graaff Facilities

Conf-770523--8

AUTHOR(S): G. F. Auchampaugh, D. M. Drake, and L. R. Veeser

SUBMITTED TO: Symposium on Neutron Data from 10 to 40 MeV
Brookhaven National Laboratory, May 3-5, 1977

The Los Alamos Scientific Laboratory requests that the publisher identify this article as work performed under the auspices of the USERDA.

los alamos
scientific laboratory
of the University of California
LOS ALAMOS, NEW MEXICO 87545

An Affirmative Action/Equal Opportunity Employer

MASTER

DISTRIBUTION OF THIS DOCUMENT IS UNLIMITED

UNITED STATES
ENERGY RESEARCH AND
DEVELOPMENT ADMINISTRATION
CONTRACT W-7405-ENG. 36

Neutron Cross Section Programs in the Energy Region from 1 to 24 MeV at the LASL Van de Graaff Facilities*

G. F. Auchampaugh, D. M. Drake, and L. R. Veeser
University of California, Los Alamos Scientific Laboratory
Los Alamos, New Mexico 87545

Neutron measurements relevant to the Los Alamos Scientific Laboratory's (LASL) programmatic efforts and to the U. S. fission and fusion energy programs can be divided into four categories: secondary neutron emission cross sections on light elements,[1] gamma-ray production cross sections,[2] total cross sections on light isotopes,[3] and (n,2n) and (n,3n) cross sections.[4] Many of these measurements have been performed using the unusual capabilities of the LASL's Van de Graaffs. This is especially true for the high-energy ($\geq$ 20 MeV) measurements on (n,2n) and (n,3n) cross sections. The purpose of this paper is to describe briefly the four types of measurements, to illustrate each measurement with some examples, and to present any new data that are not as yet available in the literature. We will also indicate in which programs new measurements are planned for the next year.

SECONDARY NEUTRON EMISSION CROSS SECTION PROGRAM

Differential elastic and inelastic cross sections and double-differential continuum cross sections have been measured for 5.9-, 10.1-, and 14.2-MeV incident neutrons on beryllium using the LASL tandem and single-ended Van de Graaff facilities. Inelastic here refers collectively to the states at 1.6-, 2.43-, 2.8-, and 3.06-MeV in ^{9}Be. Data were taken at scattering angles between 25° and 145°.

The H(t,n) reaction was used for the 5.9- and 10.1-MeV measurements instead of the customary inverse reaction because, in principle, all sources of neutron background can be investigated (the breakup neutron threshold lies above the energy region of interest at about 24 MeV) and because the H(t,n) reaction produces about a factor of 20 more neutrons in the forward direction than the inverse reaction. The H(t,n) reaction, however, does produce a sizeable, but measureable, neutron background in the continuum region from charge-particle reactions in the entrance and beam stop materials. The hollow samples were placed about 164 mm from the center of the target cell and the scattering angle changed by rotating the detector about the axis of the sample.

The ^{2}H(t,n) reaction was used for the 14.2-MeV measurements. The triton beam was stopped in the deuterium gas of the target. The samples were placed in the plane perpendicular to the beam direction about 100 mm from the target. The scattering angle was

---

*Work performed under the auspices of the United States Energy Research and Development Administration.

changed by rotating the sample in this plane about the target. In this geometry the energy of the incident neutron beam did not change with scattering angle.

The neutron detector was a NE-213 scintillator 100 mm in diameter by about 76-mm thick, which was directly coupled to the photocathode surface of an RCA-8854 photomultiplier. The bias on the detector was set to correspond to a neutron energy of approximately 300 keV. Pulse-shape discrimination using the zero-crossover technique[5] was used to reduce the gamma-ray background. The detector was located about 2.7 m from the sample inside of a massive neutron shield that consisted of paraffin impregnated with lithium hydride.

The multiple scattering correction was calculated using the LASL Monte Carlo code MCN.[6] The neutrons were tallied by emission-energy and -angle according to the type of reaction that created them: elastic, inelastic, elastic-elastic, elastic-inelastic, and inelastic-inelastic. Calculations were made on normal density and on 0.01 normal density samples at each incident neutron energy. The multiple scattering correction as a function of emission-energy and-angle was obtained by taking a ratio of the results from the different sample runs. The beryllium cross section data in the ENDF/B-IV files were used in these calculations. The corrections were nominally less than 10%.

The beryllium data were converted to cross section by normalizing the data to the hydrogen scattering data obtained from samples of polyethylene and using the Hopkins and Breit n,p scattering cross section.[7] At high energies and small scattering angles the hydrogen elastic peak was not completely resolved from the carbon elastic peak and therefore it was necessary to take data on a carbon sample to correct the polyethylene sample data for the carbon contaminant.

Since the cross section was obtained from a ratio of the beryllium data to the hydrogen data it was only necessary to measure the relative efficiency of the neutron detector. The relative efficiency of the detector was measured from 0.3 MeV to 20 MeV using the ^{2}H(d,n), ^{3}H(p,n), and ^{3}H(d,n) reactions and by elastically scattering neutrons off of hydrogen and using the n,p scattering cross section.[7]

As a self-consistency check on the elastic data, data were taken with the ^{3}H(p,n) reaction at 5.9 and 10.1 MeV. The agreement between the sets of data was better than 4%. Since the statistics in the continuum region were poor and the background very large, a meaningful comparison could not be made with the H(t,n) data. At this time we did not have the benefit of the source reaction studied[8] made at LASL that showed that the gold beam stop, which we were using, created several orders of magnitude more background than either a ^{28}Si or ^{58}Ni beam stop.

To check the multiple scattering correction we made several measurements on samples of beryllium with different dimensions. The elastic and inelastic cross sections obtained agreed to within 3% and the continuum cross sections to better than 10%.

An example of the double-differential cross sections of beryllium for 5.9-MeV incident neutrons is shown in Fig. 1. The low-energy tail on the elastic peak for $\theta_L = 125°$ is due to poor bunching of the charged particle beam and not to the 1.6-MeV state in ^{9}Be. As is apparent, there is no evidence for excitation of a level at 1.6 MeV even for our 125° data that would clearly show such a level.

It is instructive to generate energy distributions from the ENDF/B-IV cross section files to compare with our measured distributions. An example of such a comparison is shown in Fig. 2 f r 5.9-MeV neutrons. Our data are plotted as a solid line and the calculation as a short- and long-dashed line. This comparison, which is typical, clearly shows the overemphasis on the low-lying states in ^{9}Be in the ENDF/B-IV beryllium cross section file. We have also plotted (dash-dot line) the results of a statistical phase-space calculation of the energy distribution for the three-body final state configuration consisting of two neutrons and the ^{8}Be nucleus. Clearly the phase-space calculation oversimplifies the neutron production mechanism in beryllium by failing to account for the maxima in the cross sections that correspond to transitions to states in ^{9}Be.

During the next year we plan to measure the secondary neutron emission cross sections for 6-, 10-, and 14-MeV incident neutrons on ^{6,7}Li. For these measurements we will use the ^{3}H(p,n) reaction. A recent study at LASL[8] has shown that with the proper choice of beam stop and entrance materials neutron background in the continuum region from proton reactions in these materials can be several orders of magnitude less than from triton reactions in similar materials. This study also showed that the breakup process is not a serious problem for neutron energies below 10 MeV. In fact, the background from this process is comparable to that from the beam stop and entrance foil materials.

NEUTRON GAMMA-RAY PRODUCTION CROSS SECTION PROGRAM

Neutron gamma-ray production cross sections at selected angles and for 14.2-MeV neutrons have been measured for a wide range of nuclei including beryllium, carbon, niobium, magnesium, aluminum, titanium, vanadium, chromium, iron, nickel, and copper.

The data were taken at the LASL Van de Graaff using a nanosecond pulsed beam of tritons and the neutron producing reaction ^{2}H(t,n). The geometry was the same as that used for the beryllium secondary neutron emission measurements at 14 MeV. The samples were elemental disks of dimensions 6-mm thick by 44-mm diam and were located in the plane perpendicular to the beam direction about 100 mm from the target.

The gamma-ray detector was a 15.2-cm-diam by 25.4-cm-long NaI (Tl) crystal with an angular anti-Compton NaI (Tl) scintillator surrounding the main crystal. The distance between the detector and the samples was about 1 m. The time-of-flight technique (with

5-ns timing resolution) was used to sort out the desired gamma rays from neutron-induced and other background events in the crystal.

Response functions were measured with monoenergetic gamma-ray sources from 0.28 MeV to 4.4 MeV. Due to the size of the center crystal of the detector and the anti-Compton shield, the response function could be represented by a single gaussian peak with a nearly flat tail extending to zero energy at a level of approximation 1/30 of the gaussian peak height. Gamma-ray attenuation in the sample required a correction to the measured response functions, which was determined experimentally by placing monoenergetic gamma-ray sources behind standard absorbers (for example, iron) at the sample position and varying the thickness of the absorbers.

The neutron flux was calculated from the geometry of the system, triton beam current, deuteron gas pressure and the appropriate ^{2}H(t,n) cross section[9] and confirmed by direct measurements of the flux using a proton-recoil telescope and the Hopkins and Breit n,p cross section.[7] The measurements agreed to ± 5% with the neutron-flux calculation.

Differential gamma-ray production cross sections were measured from 0.2-MeV to 9.0-MeV gamma-ray energy for the elements listed in Table I at the angles indicated by an x. Differential gamma-ray cross sections for prominent gamma rays produced in the neutron reaction were measured for the elements listed in Table II. Beryllium is a special case because all of its known excited states are particle unstable and the ^{9}Be(n,n'γ) reaction is improbable. The only gamma ray observed in the beryllium measurement was that for the 480-keV first excited state in ^{7}Li that is formed by the ^{9}Be(n,t)^{7}Li* reaction.

TABLE I

List of differential gamma-ray production cross sections that have been measured at LASL for neutrons of 14.2 MeV. The x indicates the measurement angle.

ELEMENT	ANGLE			
	90°	110°	120°	130°
Magnesium	x	x		x
Aluminum	x	x		x
Titanium	x	x		x
Vanadium	x	x		x
Chromium	x	x		x
Iron	x	x		x
Nickel			x	
Copper		x		
Niobium	x	x		x

TABLE II

List of differential gamma-ray cross sections for prominent gamma rays that have been measured at LASL for neutrons of 14.2 MeV. The x indicates the measurement angle.

ELEMENT	GAMMA-RAY ENERGY (MeV)	ANGLE						
		45°	64°	90°	110°	120°	125°	130°
Beryllium	0.48			x				
Carbon	4.43	x	x	x	x		x	x
Magnesium	1.37			x	x			x
Aluminum	0.84+1.01			x	x		x	x
	1.7 +1.8			x	x		x	x
	2.2			x	x		x	x
	3.0			x	x		x	x
Chromium	1.33+1.43			x	x	x		x
Iron	0.85			x	x		x	x
	1.24			x	x		x	x

An example of the type of data available is given in Table III for Iron. The data are tabulated in 0.1-MeV energy bins from 0.2 MeV to 4.0 MeV and in 0.5-MeV bins from 4.0 MeV to 9.0 MeV. The cross sections are averages over these energy bins. The uncertainty on each datum point represents a quadruture of the statistical uncertainty and the systematic uncertainty. The various sources of systematic errors and the uncertainties used in calculating the total uncertainty are listed in Table IV. The gamma-ray production cross sections on iron at 90° (o) and at 120° (x) are plotted in Fig. 3. The solid curve is a calculation of the gamma-ray production cross section based upon the ENDF/B-IV cross sections assuming that the gamma rays are emitted isotropically.

There are no plans to measure additional gamma-ray production cross sections at 14 MeV.

TABLE III

Iron Gamma-Ray Production Cross Sections as a Function of Gamma-Ray Energy

Energy Interval (MeV)	90°		Energy Interval (MeV)	90°	
	σ ±	Δσ (mb/sr)		σ ±	Δσ (mb/sr)
0.2 - 0.3	10.4	4.5	3.0 - 3.1	2.4	.3
0.3 - 0.4	11.7	4.7	3.1 - 3.2	2.0	.2
0.4 - 0.5	10.2	2.7	3.2 - 3.3	2.3	.2
0.5 - 0.6	6.3	.7	3.3 - 3.4	1.9	.2
0.6 - 0.7	4.3	.5	3.4 - 3.5	2.0	.2
0.7 - 0.8	15.3	1.5	3.5 - 3.6	2.2	.3
0.8 - 0.9	38.6	3.7	3.6 - 3.7	2.0	.2
0.9 - 1.0	14.9	1.5	3.7 - 3.8	1.7	.2
1.0 - 1.1	7.4	.7	3.8 - 3.9	1.6	.2
1.1 - 1.2	9.8	1.0	3.9 - 4.0	1.14	.15
1.2 - 1.3	19.8	2.0	4.0 - 4.5	1.28	.17
1.3 - 1.4	13.3	1.3	4.5 - 5.0	1.07	.15
1.4 - 1.5	5.8	.6	5.0 - 5.5	.92	.14
1.5 - 1.6	3.4	.4	5.5 - 6.0	.95	.15
1.6 - 1.7	3.9	.4	6.0 - 6.5	1.03	.17
1.7 - 1.8	5.0	.5	6.5 - 7.0	.90	.15
1.8 - 1.9	4.9	.5	7.0 - 7.5	.61	.12
1.9 - 2.0	3.9	.4	7.5 - 8.0	.63	.12
2.0 - 2.1	3.2	.3	8.0 - 8.5	.40	.09
2.1 - 2.2	3.2	.3	8.5 - 9.0		
2.2 - 2.3	2.8	.3			
2.3 - 2.4	2.8	.3			
2.4 - 2.5	2.7	.3			
2.5 - 2.6	3.4	.4			
2.6 - 2.7	3.5	.4			
2.7 - 2.8	2.6	.3			
2.8 - 2.9	2.1	.2			
2.9 - 3.0	2.2	.2			

TABLE IV

Systematic Uncertainties in the Differential Gamma-Ray Production Cross Sections

Type	Uncertainty (Percent)	
Gamma-ray efficiency	± 3	0.2 to 3 MeV
	±12	at 9 MeV
Unfolding	± 5	
Neutron multiple scattering	± 2.5	
Flux	± 7	
Sample position	± 2	
TOTAL	± 9.7	0.2 to 3 MeV
	±15.1	at 9 MeV

LIGHT ELEMENT TOTAL CROSS SECTION PROGRAM

High-resolution and high-accuracy total cross sections of ^{9}Be, ^{10,11}B and ^{12,13}C have been measured from 1.0 to 14 MeV. The LASL tandem accelerator was used to produce a "white" source of neutrons by stopping a pulsed beam of 15-MeV deuterons in a thick beryllium target. The deuteron pulses occurred every 3.2 μs and produced an average current on target of between 160 and 400 namps.

Two NE-110 plastic scintillator detectors were used for the measurements. Both pieces of plastic were machined to fit the curvature of the photocathode surface of an RCA-8854 photomultiplier tube. The carbon and beryllium data were taken with a scintillator 12.5 cm in diameter with a center thickness of 2.2 cm. The boron data were taken with a scintillator 10 cm in diameter with a center thickness of 1.2 cm. The electronics of this detector was designed to take advantage of the less than 1-ns deuteron pulse width available from the accelerator. However, the deuteron beam could not be bunched to less than about 1.8 ns for these measurements and therefore the boron data have poorer resolution than the other data.

The open beam counting rate for the thicker detector at 400 namps was approximately 20000 per second.

The overall resolution of the detector system as measured by the width of the gamma-ray peak that occurred at zero time and by the widths of narrow resonances in ^{16}O and ^{18}O was 1.8 $\pm$ 0.1 ns (2.0 $\pm$ 0.1 ns) for the thicker (thinner) detector. This timing uncertainty is equal to an energy uncertainty in keV of 1.3 (1.4)$E^{3/2}$ with E measured in MeV for our flight path of 38.9 m.

Since the resolution of the system was less than 2 ns the data were recorded in channel widths of 0.5 ns.

The accuracy of the neutron energy scale is given by $\pm$ 0.070 E $\sqrt{1.79E+0.75}$ with E measured in MeV. This means, for example, that the energy of the narrow resonance in ^{12}C at 2.077 MeV has an uncertainty of less than ± 260 eV.

The data were corrected for backgrounds that varied from 3% of the open beam spectrum at 1.5 MeV, 0.5% at 4 MeV, to 1% at 14 MeV.

The systematic uncertainty in the transmission is estimated to be ± 1.7%. This uncertainty is determined from a quadruture of the following estimates of the various sources of errors: sample thickness ± 0.7%, background ± 1%, normalization ± 1%, and dead-time ± 0.5%. Since the fractional uncertainty in the cross section is equal to the fractional uncertainty in the transmission multiplied by $1/n\sigma$, the systematic uncertainty in the cross section is somewhat larger because, for our samples, $n\sigma$ was generally less than one.

As an example of the data obtained with the Be(dn,N) reaction we present the total cross section of ^{11}B from 1.0 to 14 MeV in Figs. 4-6. The cross section has been corrected for the ^{10}B isotopic impurity present in the sample. The data from 1.0 to 1.5 MeV in Fig. 4 and 4.0 to 14 MeV in Fig. 6 have been averaged over five channels. Note the suppresssed zero origin on the vertical scale in Fig. 6. This was done to reveal the fine structure present in the data that could only be seen with high statistical accuracy data. The statistical uncertainty in the cross section varies from a few percent at 1.5 MeV to about 0.5 percent at 9 MeV to about 1 percent at 14 MeV. These data required about six hours of machine time.

There are no plans to continue the light element total cross section program at the Van de Graaff because a time-of-flight facility is being built at the Los Alamos Meson Facility that will have a potential for much higher energy resolution than the Van de Graaff facility.

(n,2n) AND (n,3n) CROSS SECTION PROGRAM

(n,2n) and (n,3n) cross sections for $^{6,7}Li$, Be, Ti, V, Cr, Mn, Fe, Co, Ni, Cu, and Nb have been measured from 14.7 to 24 MeV using the LASL Van de Graaff and a large gadolinium-loaded liquid scintillator tank to detect the neutrons.

The neutrons were produced by the $^{3}H(d,n)$ reaction. The deuteron beam was chopped into pulses 1-μs wide at a repetition rate of 25 kHz. The current was adjusted to keep the average number of (n,xn) reactions per burst much less than one, thus minimizing the correction for multiple events in any single burst.

The detector was a 75-cm-diam tank filled with 200 ℓ of NE 323 that was loaded with 0.5% by weight gadolinium. The tank was located 2.6 m from the source in a well-shielded room. It was viewed by eight photomultiplier tubes (type RCA 4522) divided into two banks of four tubes each. A coincidence was required between the two banks to reduce events from tube noise. Since the capture half life of neutrons in the tank was much longer than the response time of the electronics, individual neutron events could be resolved. A fast scaler gated on for 23 μs counted the number of tank pulses per beam pulse and a computer sorted them out according to the number detected.

The neutron flux was measured by a 5.1-cm-long by 5.1-cm-diam cylinder of NE-213 liquid scintillator mounted on an RCA-8575 photomultiplier and located 4.7 m behind the sample. The pulse height was recorded during each run and the neutron flux was found by relating the height and end point of the plateau from the recoil protons to the absolute differential efficiency measurements of Verbinski.[10]

The neutron efficiency of the tank was measured by a ^{252}Cf source on a solid state detector placed at the center of the tank. Corrections were applied to the measured efficiency for differences between the Cf fission neutron spectrum shape and the (n,2n) and (n,3n) spectra shapes. The (n,xn) shapes were calculated using a statistical model that included preequilibrium neutron emission.[4]

The data were corrected for backgrounds and for losses of tank pulses that occurred during the deadtime associated with each pulse. Since the probability for two single events occurring during a gate was not negligible compared with the number of true (n,2n) events, a multiple-event correction was applied to each sample run. A similar correction to the (n,3n) data was negligible. The final correction, which varied with the incident neutron energy and with the multiplicity of the(n,xn) reaction, removed the effects of detector efficiency to give the multiplicities of neutrons emitted from the target.

Preliminary results on the (n,2n) cross sections of Be, Ti, V, Cr, Mn, Fe, Ni, and Cu are listed in Table V. The measured (n,3n) cross sections are essentially zero up to 21 MeV. The uncertainty given for each cross section represents a quadruture of the statistical uncertainty and a systematic uncertainty that varied from 3 to 6%. The ^{6,7}Li(n,2n) cross sections are both about 100 mb and roughly constant between 14.7 and 21 MeV except that ^{7}Li drops off to about 80 mb at 14.7 and 16 MeV. When the final results become available, the 21-MeV cross sections in the table will probably go up by about 5 to 10%, the 18-MeV ones should remain unchanged, and the 14.7-MeV ones may go down 3 to 5%. The Be data have already been roughly corrected.

The data on Nb and Co are tabulated in ref. 4. The (n,2n) and (n,3n) cross sections for Nb are plotted on Fig. 7. The data of Frehaut et al.[11] are represented by the closed circles and our data by the open circles (n,2n) and open triangles (n,3n). The solid line represents a calculation of the (n,xn) cross sections using a statistical model that includes preequilibrium neutron emission.

Since we have measured (n,xn) cross sections for most available materials, no additional measurements are planned for the next year.

TABLE V

Preliminary (n,2n) Cross Sections

E (MeV)	Be	Ti	V	Cr	Mn	Fe
6.0	0.545±0.042					
14.7	0.472±0.026	0.51±0.03	.66±.04	.47±.03	.85±.05	.50±.04
16	0.475±0.041	0.58±0.04	.70±.06	.53±.04	.89±.05	.56±.05
17	0.431±0.038	0.63±0.03	.77±.05	.65±.03	.85±.04	.59±.03
18	0.422±0.035	0.67±0.04	.82±.06	.68±.04	.85±.04	.68±.04
19	0.365±0.033	0.65±0.03	.79±.05	.65±.03	.81±.04	.64±.04
20	0.389±0.033	0.65±0.03	.74±.04	.64±.03	.80±.04	.64±.04
21	0.378±0.035	0.65±0.03	.78±.04	.63±.03	.75±.04	.60±.04

E (MeV)	Ni	Cu
14.7	.20±.02	.74±.04
16	.23±.02	.87±.05
17	.26±.03	.79±.04
18	.26±.02	.86±.05
19	.25±.02	.79±.04
20	.27±.02	.82±.04
21	.27±.02	.76±.04

REFERENCES

1. D. M. Drake, G. F. Auchampaugh, E. D. Arthur, C. E. Ragan, and P. G. Young, Los Alamos Scientific Laboratory Report, LA-6257, 1976. Accepted for publication in Nucl. Sci. and Eng.
2. D. M. Drake, E. D. Arthur, and M. G. Silbert, accepted for publication in Nucl. Sci. and Eng., 1977.
3. G. F. Auchampaugh, C. E. Ragan, S. Plattard, and N. W. Hill, Los Alamos Scientific Laboratory Report, LA-6761, 1977.
4. L. R. Veeser, E. D. Arthur, and P. G. Young, to be published, 1977.
5. T. K. Alexander and F. S. Goulding, Nucl. Instrum. Methods 13, 244 (1961).
6. E. D. Cashwell, J. R. Neegaard, W. M. Taylor, and G. D. Turner, Los Alamos Scientific Laboratory Report, LA-4751, 1972.

7. J. C. Hopkins and G. Breit, *Nucl. Data Tables* *A9* 137 (1971).
8. M. Drosg, G. F. Auchampaugh, and F. Gurule, *Nucl. Instrum. Method* *140*, 515 (1977).
9. J. E. Brolley, Jr., and J. L. Fowler, *Fast Neutron Physics, Part I*, p. 94, Interscience Publishers Inc., New York, 1960.
10. V. V. Verbinski, W. R. Burrus, T. A. Love, W. Zobel, and N. W. Hill, *Nucl. Instrum. Method* *65*, 8 (1968).
11. J. Frèhaut and G. Mosinski, *Nuclear Cross Sections and Technology*, NBS Spec. Publ. 425, Vol. II, 1975.

FIGURE CAPTIONS

Fig. 1. Double-differential cross sections for 5.9-MeV incident neutrons on beryllium. The cross sections are given in the laboratory system. The arrows indicate the positions of the low-lying states in ^{9}Be, which may contribute to the observed maxima in the cross sections at the indicated energies. The low-energy shoulder on the elastic peak $\theta_L = 125°$ is due to poor bunching of the charged particle beam.

Fig. 2. Comparison of beryllium double-differential cross sections for a laboratory angle of 80°, and an incident neutron energy of 5.9 MeV. Our data are plotted as a solid line, the ENDF/B data as a short and long dash line, and the unnormalized three-body phase-space calculation as a dashed line.

Fig. 3. Spectrum of gamma rays observed from iron, circles and crosses representing angles of 90° and 120° respectively, compared to the ENDF/B-IV file (histogram).

Fig. 4. Total cross section of ^{11}B from 1.0 MeV to 4 MeV. The data below 1.5 MeV have been averaged over five channels.

Fig. 5. Total cross section of ^{11}B from 4.0 MeV to 9.0 MeV.

Fig. 6. Total cross section of ^{11}B from 4 MeV to 13.9 MeV. Note the suppressed zero origin on the vertical scale. The data have been averaged over five channels.

Fig. 7. Cross sections for ^{93}Nb (n,xn). The closed circles are from Ref. 11, the open circles are our (n,2n) results, the open triangles are our (n,3n) results, and the solid line is a statistical model calculation of the (n,xn) cross sections.

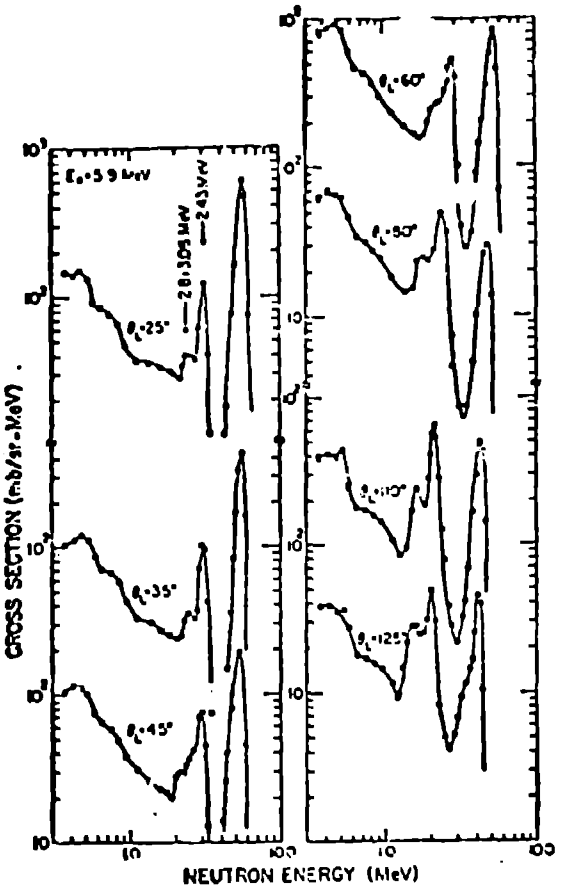
CROSS SECTION (mb/sr-MeV)
NEUTRON ENERGY (MeV)
E_p=5.9 MeV
28.3 MeV
24.3 MeV
θ_L=25°
θ_L=35°
θ_L=45°
θ_L=60°
θ_L=90°
θ_L=110°
θ_L=125°
10
100

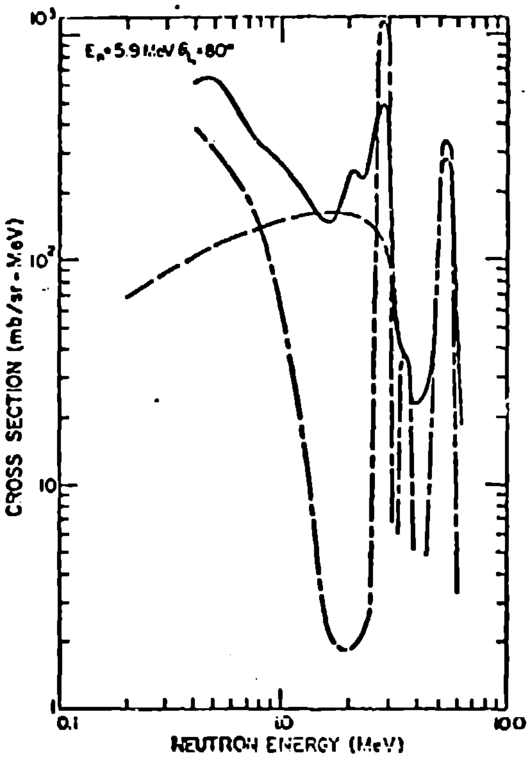
E_p=5.9 MeV θ_L=80°
CROSS SECTION (mb/sr-MeV)
NEUTRON ENERGY (MeV)
10^3
10^2
10
1
0.1
10
100

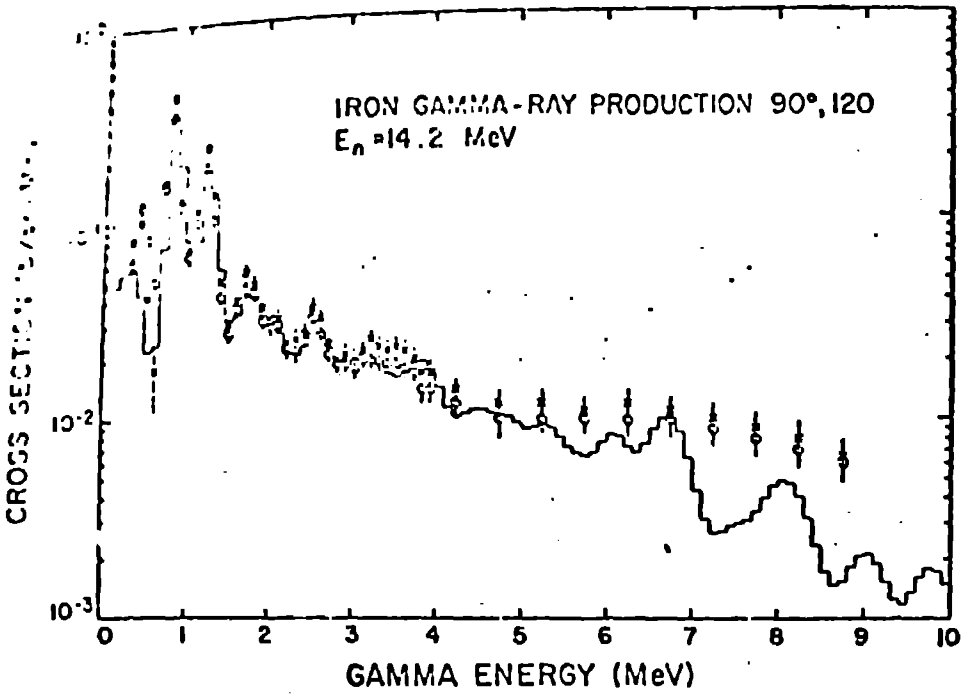
IRON GAMMA-RAY PRODUCTION 90°, 120
E_n =14.2 MeV
CROSS SECTION
10^{-2}
10^{-3}
0
1
2
3
4
5
6
7
8
9
10
GAMMA ENERGY (MeV)

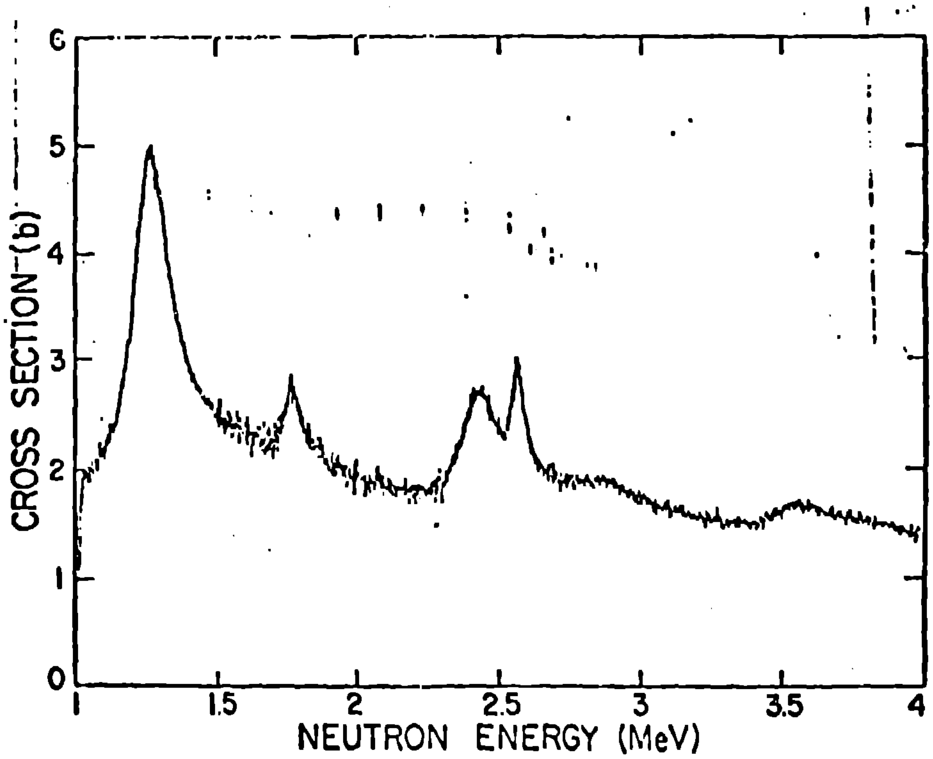
CROSS SECTION (b)
0
1
2
3
4
5
6
1
1.5
2
2.5
3
3.5
4
NEUTRON ENERGY (MeV)

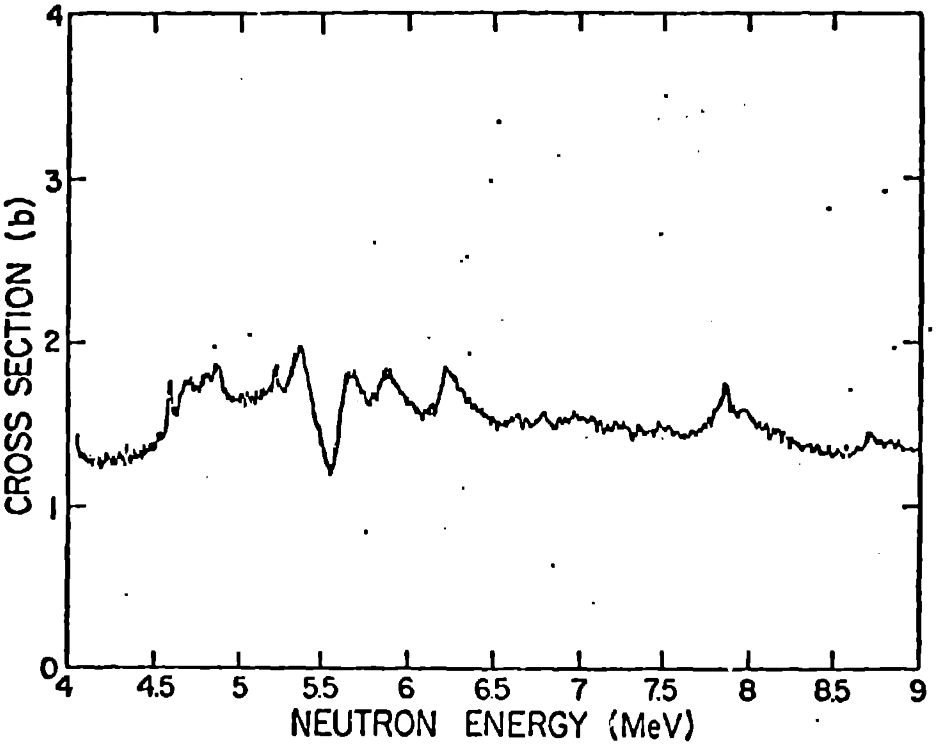
CROSS SECTION (b)
NEUTRON ENERGY (MeV)
0
1
2
3
4
4
4.5
5
5.5
6
6.5
7
7.5
8
8.5
9

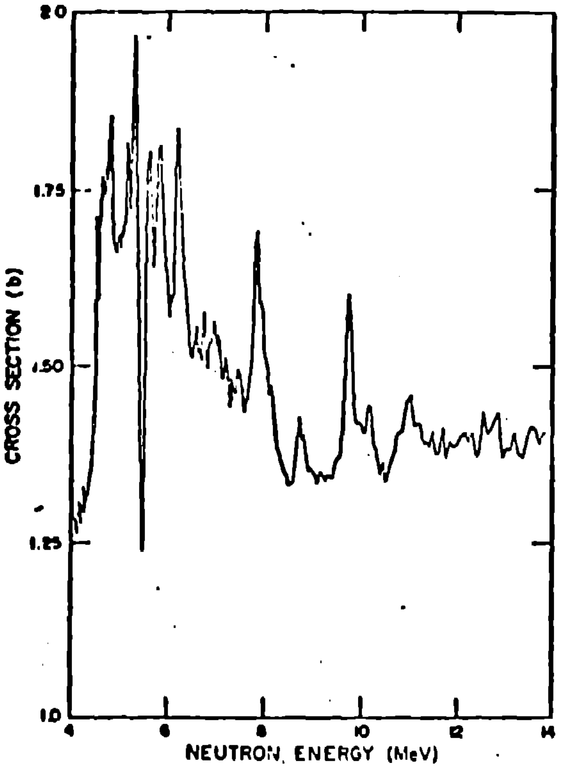
CROSS SECTION (b)
NEUTRON ENERGY (MeV)
1.0
1.25
1.50
1.75
2.0
4
6
8
10
12
14

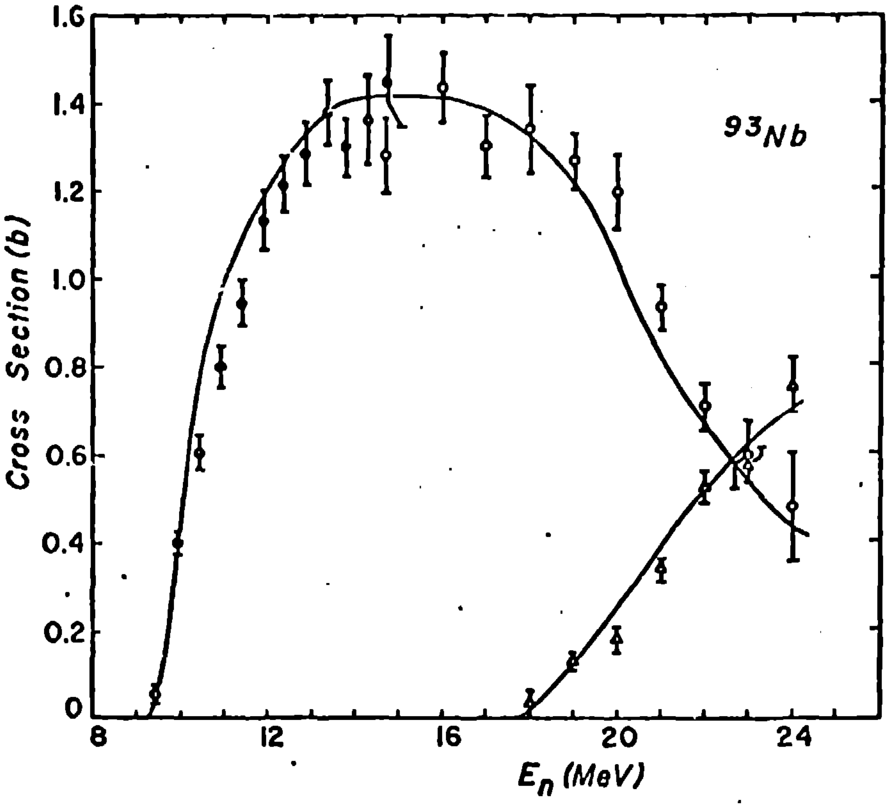

^{93}Nb
Cross Section (b)
1.6
1.4
1.2
1.0
0.8
0.6
0.4
0.2
0
8
12
16
20
24
E_n (MeV)